chemistry. Although dehydrogenation predominates, products arising from C-C insertion are observed for alkanes larger than propane, particularly in the secondary reactions. The Sc_4^+ cluster is observed to sequentially add 2 oxygen atoms from dioxygen and 8 sulfur atoms from ethylene sulfide. In addition to dehydrogenating benzene, formation of ring cleavage products affirms the highly reactive nature of Sc_4^+. Finally this work demonstrates that the laser ionization-cavity source holds promise as a convenient and clean method of generating metal cluster ions for further study by FTMS.

Acknowledgment is made to the Division of Chemical Sciences in the Office of Basic Energy Sciences in the United States Department of Energy (DE-AC02-80ER10689) and the National Science Foundation (CHE-8310039) for supporting the advancement of FTMS methodology.

Registry No. Sc_4^+, 94669-91-7; methane, 74-82-8; ethane, 74-84-0; propane, 74-98-6; butane, 106-97-8; 2-methylpropane, 75-28-5; pentane, 109-66-0; 2,2-dimethylpropane, 463-82-1; 2-methylbutane, 78-78-4; hexane, 110-54-3; butane-*1,1,1,4,4,4-d*$_6$, 13183-67-0; oxygen, 7782-44-7; benzene, 71-43-2; methanol, 67-56-1; ethylene sulfide, 420-12-2.

Kinetics of the $Cr(CO)_6$ and $W(CO)_6$ Catalyzed Water Gas Shift Reaction: Photoinitiated Formate Decomposition as a Probe of the Catalytic Cycle

Bruce H. Weiller, Jian-Ping Liu,† and Edward R. Grant*

Contribution from the Department of Chemistry, Baker Laboratory, Cornell University, Ithaca, New York 14853. *Received September 4, 1984*

Abstract: The catalytic cycle for the water gas shift reaction is initiated under mild conditions (5-65 °C) by the pulsed laser (337 nm) irradiation of $M(CO)_6$ (M = Cr, W) in basic water/methanol solution. CO is supplied to the reaction as NaO_2CH. The cycle displays conventional saturation behavior in formate substrate concentration. The formate saturated rate (R_{max}) is enhanced by visible irradiation and is sensitive to deuterium substitution in formate (R^H_{max}/R^D_{max} = 3.4 ± 0.9 and 4.4 ± 0.2 for Cr and W, respectively, at 25.0 °C). No CO inhibition in the catalytic cycle is observed, but the rate is inhibited by increasing water concentration. These observations are interpreted in terms of reversible reactions with H_2O that preceed both entry into the cycle and rate-limiting decarboxylation/hydride migration within the cycle. Activation energies for the cycle are 26.0 ± 1.4 and 24.8 ± 0.8 kcal mol^{-1} for Cr and W, respectively, and are attributed to the decarboxylation step. Rate constants for formate binding and decarboxylation along with equilibrium constants for water reactions are reported. This work demonstrates the impotance of water as a coordinating ligand in the water gas shift catalytic cycle.

The water gas shift reaction (WGSR)

$$CO + H_2O \rightarrow H_2 + CO_2 \quad (1)$$

figures importantly in manufacturing practice, both as a means for the enrichment of synthesis gas streams in H_2 and as a side reaction of significance in hydroformylation and Fischer-Tropsch processes.[1] In industry water gas shift is promoted by heterogeneous catalysts, typically Fe_2O_3, at high temperature and pressure ($T \approx 400$ °C, $P \approx 30$ atm).[2] However, several homogeneous systems exist that require less severe conditions.[3] Among these are laboratory systems based on the groups 6 and 8 metal carbonyls.

The properties of the group 6 systems are of particular interest because in basic water-methanol solution, catalysis apparently proceeds via a formate complex[4] analogous to surface-bound formates observed in heterogeneous water gas shift.[5] A resistance to sulfur poisoning adds further significance to this homogeneous system.[6]

The kinetics of thermally initiated catalysis of the water gas shift reaction by group 6B metal carbonyls has been thoroughly studied by King and co-workers.[4a] They find the mechanism in Scheme I to be consistent with the data. Hydrogen evolution in this system is observed to follow a simple rate law

$$\frac{d[H_2]}{dt} = \frac{k_a k_b}{k_{-a}} \frac{[HCO_2^-][M(CO)_6]}{[CO]} \quad (2)$$

The form of this expression for the rate of a catalytic process is significant. By explicitly including terms in $[HCO_2^-]$ and [CO],

Scheme I

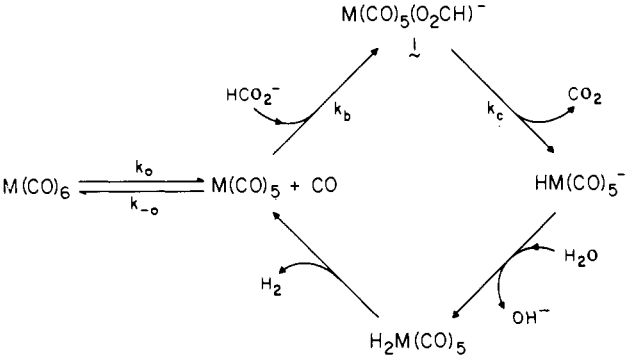

it emphasizes competitive CO dissociation/rebinding and reaction with formate by the metal complex in the *initiation* of the catalytic cycle. However, as evidenced by the absence of a term yielding saturation in formate, neither the method nor the kinetic analysis

† Permanent address: Department of Chemistry, Hua Zhong Normal University, Wuhan, Hubei, People's Republic of China.

(1) Keim, W., Ed. "Catalysis in C_1 Chemistry"; D. Reidel Publishing Co.: Dordrecht, 1983; pp 50 and 136.
(2) Satterfield, C. N. "Heterogeneous Catalysis in Practice"; McGraw-Hill: New York, 1980; p 292.
(3) Ford, P. C. *Acc. Chem. Res.* **1981**, *14*, 31 and references therein.
(4) (a) King, A. D.; King, R. B.; Yang, D. B. *J. Am. Chem. Soc.* **1981**, *103*, 2699. (b) Slegeir, W. A. R.; Sapienza, R. S.; Rayford, R.; Lam, L. *Organometallics* **1982**, *1*, 1728. (c) Attali, S.; Mathieu, R.; Leigh, G. J. *J. Mol. Catal.* **1982**, *14*, 293.
(5) (a) Rubene, N. A.; Davydov, A. A.; Kravstov, A. V.; Usheva, N. V.; Smol'yaninov, S. I. *Kinet. Catal. (Engl. Transl.)* **1976**, *17*, 400. (b) Tamaru, K. "Dynamic Heterogeneous Catalysis"; Academic Press: New York, 1978; p 121.
(6) King, A. C.; King, R. B.; Yang, D. B. *J. Chem. Soc., Chem. Commun.* **1980**, 529.

0002-7863/85/1507-1595$01.50/0

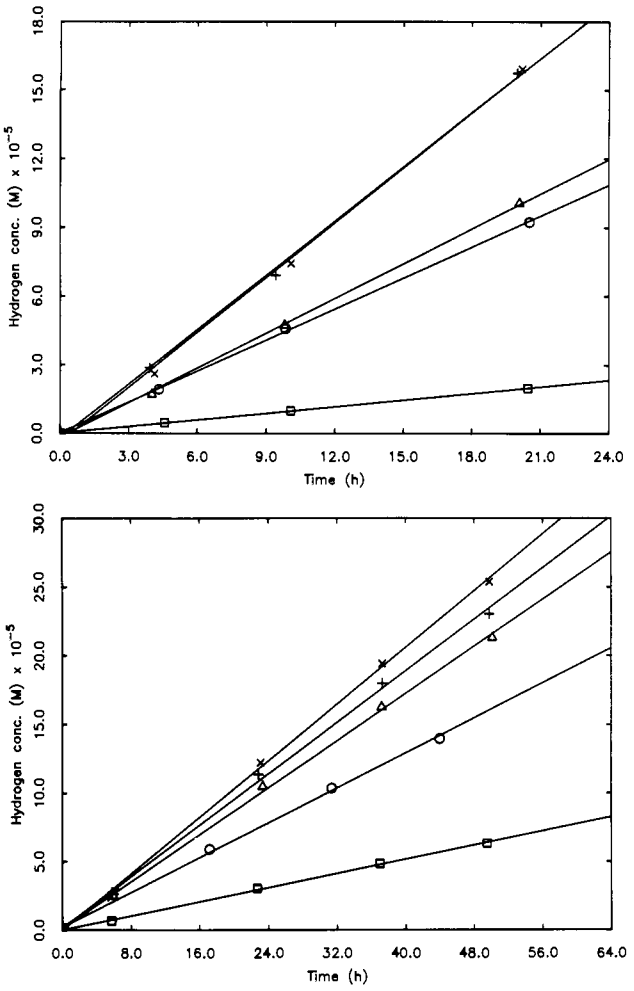

Figure 1. Hydrogen production for various formate concentrations at 25.0 °C: (a, top) $Cr(CO)_6$—(□) $[NaO_2CH] = 6.95 \times 10^{-3}$, (○) $[NaO_2CH] = 3.48 \times 10^{-2}$, (△) $[NaO_2CH] = 6.95 \times 10^{-2}$, (+) $[NaO_2CH] = 0.1153$, (×) $[NaO_2CH] = 0.1756$; (b, bottom) $W(CO)_6$—(□) $[NaO_2CH] = 7.10 \times 10^{-3}$, (○) $[NaO_2CH] = 3.55 \times 10^{-2}$, (△) $[NaO_2CH] = 7.10 \times 10^{-2}$, (+) $[NaO_2CH] = 9.69 \times 10^{-2}$, (×) $[NaO_2CH] = 0.1805$. The hydrogen concentration is calculated by dividing the moles measured by the volume of solution (10.0 mL).

of King and co-workers is highly sensitive to the details of rate processes within the cycle itself.[7]

This is further evidenced by comparison with the work of Darensbourg and Rokicki,[8] who isolated the key decarboxylation step of the intermediate formate complex (1) by anhydrous dissociation of the synthetic compound. They showed on the basis of CO inhibition and isotope scrambling that CO loss is a prerequisite to decarboxylation, viz.

$$M(CO)_5(O_2CH)^- \overset{-CO}{\rightleftharpoons} M(CO)_4(O_2CH)^- \overset{-CO_2}{\rightleftharpoons} HM(CO)_4^- \quad (3)$$

The present paper reports a study of the kinetics of the group 6 carbonyl-catalyzed water gas shift reaction that focusses on the rate processes within the catalytic cycle. To isolate these critical steps of the catalytic turnover, we supply CO substrate as HCO_2^- and initiate the reaction by photolytic conversion of the precatalyst, $M(CO)_6$. This approach extends the range of catalytic activity to room temperature and below and allows us to characterize the cycle's saturation in formate. We observe direct kinetic evidence for reversible decoordination, in our case that of H_2O, preceding decarboxylation.

(7) Indeed, measured activation energies for catalytic hydrogen production correspond to the bond enthalpies for primary M–CO thermolysis (see below in text).

(8) Darensbourg, D. J.; Rokicki, A. *Organometallics* **1982**, *1*, 1685.

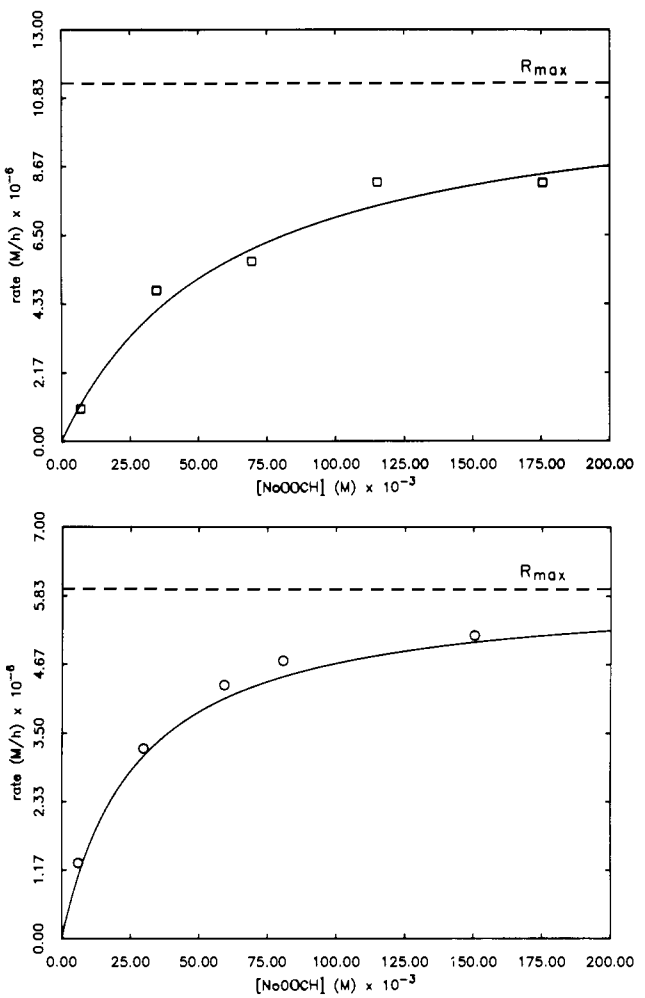

Figure 2. Rate of hydrogen production as a function of formate concentration at 25.0 °C: (a, top) $Cr(CO)_6$ and (b, bottom) $W(CO)_6$. The data are from the same experiments as those for Figure 1. The asymptotic limit is termed R_{max}.

Our results establish by means of a significant H/D isotope effect that hydride migration accompanying decarboxylation is rate determining in the formate saturated cycle. Indications are that solvent coordination plays an active role in all kinetic steps involving formally unsaturated intermediates.

We report elementary rate constants for the association (solvent displacement) reaction of formate with catalyst and for unimolecular decarboxylation. For the latter of these we establish energetic requirements in the form of Arrhenius parameters independent of hexacarbonyl dissociative initiation. We also obtain constants for key equilibria preceding (1) entry by the photolytically prepared catalyst into the cycle and (2) decarboxylation.

Results

The kinetics of the photoinitiated group 6 carbonyl-catalyzed water gas shift cycle are investigated by examining the rate of hydrogen evolution as a function of the composition of the system. We vary the concentrations of substrates HCO_2^- and H_2O, finding normal saturation behavior in formate but inhibition by water. Results to follow also show that the turnover rate of the cycle is not affected by an overpressure of CO, but it is accelerated by visible irradiation.

Formate Saturation. Once initiated by irradiation no longer than 5 min, catalysis continues indefinitely (monitored up to 7 days) at room temperature in the dark. Figure 1 shows hydrogen evolved as a function of time at 25.0 °C for various formate concentrations. When the rate is plotted against formate concentration, normal saturation behavior is observed, as can be seen in Figure 2. The asymptotic limit of the rate with respect to formate concentration is termed R_{max} and can be determined

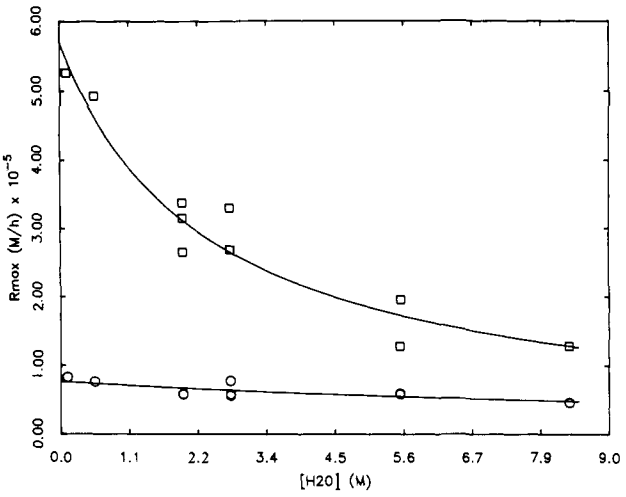

Figure 3. Water dependence of R_{max} at 25.0 °C for $Cr(CO)_6$ (□) and $W(CO)_6$ (○). R_{max} is the asymptotic limit of the rate of hydrogen evolution with respect to formate concentration (see Figure 2).

Table I. Kinetic Data for CO-Induced Reversion of Active Catalyst to $M(CO)_6$

precatalyst[a]	time, h	ln $[A/A_0]$[b]	k,[c] h^{-1}
$Cr(CO)_6$	0.00	0.00	0.105 ± 0.002
	1.83	−0.148	
	4.48	−0.431	
	8.03	−0.864	
	12.52	−1.34	
	23.97	−2.47	
$W(CO)_6$	0.00	0.00	0.0417 ± 0.0002
	3.30	−0.115	
	8.50	−0.326	
	20.98	−0.875	
	30.71	−1.28	
	44.83	−1.85	

[a] Precatalyst concentrations are $[Cr(CO)_6] = 4.79 \times 10^{-4}$ M and $[W(CO)_6] = 4.50 \times 10^{-4}$ M. [b] Absorbances are measured at the maxima of 432 and 408 nm for Cr and W, respectively. [c] k is the pseudo-first-order rate constant for the process $M(CO)_{6-n}L_n + nCO \xrightarrow{k} M(CO)_6 + nL$.

analytically (see below). When NaO_2CD is used as substrate in D_2O/CH_3OD solvent, significant isotope effects are observed. $R^H_{max}/R^D_{max} = 3.4 \pm 0.9$ and 4.4 ± 0.2 for Cr and W, respectively, at 25.0 °C.

Water Dependence. The second substrate for the WGSR is water. Rather than showing a higher rate with increased water concentration, however, the evolution of H_2 is apparently inhibited by H_2O. As shown by Figure 3, *R_{max} values at 25 °C for Cr and W depend inversely on water concentration over a range from near zero (0.11) to 8.3 M.* The dependence is strong for Cr, as R_{max} changes by more than a factor of 4, while for W the effect is a smaller 50%.

CO Dependence. Reaction 3 suggests the possibility of a CO-inhibited decarboxylation within the catalytic cycle for WGSR. To test for this effect we pressurize H_2-producing samples with CO. An ancillary process is readily observed under these conditions. The catalyst concentration steadily diminishes as the presence of excess CO drives photoprepared active complexes back to $M(CO)_6$. This is evidenced by the loss of yellow $M(CO)_{6-n}L_n$ and the growth of UV absorption bands attributed to $M(CO)_6$. By following the kinetics of hydrogen evolution, we find that an overpressure of CO does cause H_2 production to cease (Figure 4). However, Table I shows that the decay of $M(CO)_{6-n}L_n$ is pseudo first order, and the exponential decay of active catalyst, determined by this time-dependent visible absorption, must be used to correct the reaction rate in order to isolate any CO inhibition within the cycle. The product evolution curve corrected for reversion of catalyst to $M(CO)_6$ is shown in Figure 4. We see that when the rate is corrected for catalyst concentration no further

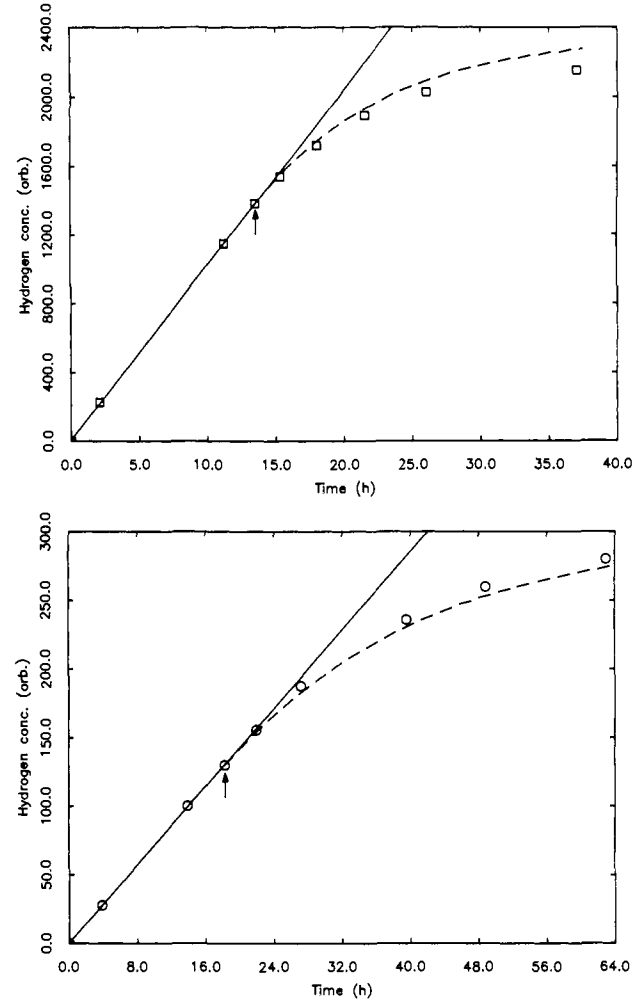

Figure 4. Effect of CO on hydrogen production at 25.0 °C: (a, top) $Cr(CO)_6$ and (b, bottom) $W(CO)_6$. The initial straight lines are the base rates prior to the addition of CO. The arrows indicate the points at which CO is added. CO causes reversion of the active catalyst back to hexacarbonyl, the rate of which can be quantitated by UV–vis absorption (see Table I). The curved line is the predicted hydrogen evolution curve with the data of Table I to correct the rate for reduced catalyst concentration.

inhibition is observed. This indicates that *the WGSR catalytic cycle itself is not inhibited by CO and that reaction 3 is not important in this system.*

Photoacceleration. To further test for a dissociative step in the catalytic cycle, we have explored the effect of visible light on hydrogen production. Substituted metal carbonyls are known to lose the most weakly bound ligand upon irradiation.[9] The hexacarbonyls absorb only in the UV, and only $M(CO)_{6-n}L_n$ species absorb in the visible. Figure 5 shows the effect of broad-band visible irradiation on active H_2-producing systems. The rate is increased by factors of 1.4 and 2.1 for Cr and W, respectively. When the light is removed, the system returns to the previous rate.[10] Visible light has no effect without prior UV irradiation. Thus we conclude that the *rate of H_2 production is photoaccelerated with visible light.*

Temperature Dependence. Within the range 5–65 °C in which no thermal initiation takes place, we find that the rate of pho-

(9) Geoffrey, G. L.; Wrighton, M. S. "Organometallic Photochemistry"; Academic Press: New York, 1979; p 70.

(10) Note that temperature increases far outside the thermostated range would be required to account for the enhancements thermally. The rate following photoacceleration for Cr is slightly lessened compared with the base rate before visible irradiation whereas for W the two rates are identical. In other experiments we observe loss of catalytic activity that is also more pronounced for Cr. We believe that both of these observations can be attributed to the consumption of catalyst by the formation of a dinuclear species (see text).

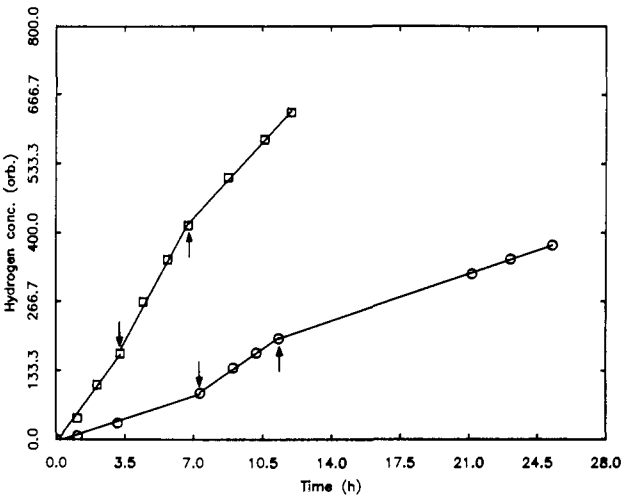

Figure 5. Photoacceleration of hydrogen production with visible light at 25.0 °C for $Cr(CO)_6$ (□) and $W(CO)_6$ (○). The arrows mark the times when the lamp is turned on and off. For both, the first three points establish the base rate in the dark. The following three points are under continuous visible ($350 < \lambda < 500$ nm) irradiation, and the last three are in the dark. Under visible irradiation the rate is 1.4 and 2.1 times the base rate for $Cr(CO)_6$ and $W(CO)_6$, respectively. The temperature is constant to ±0.3 °C.

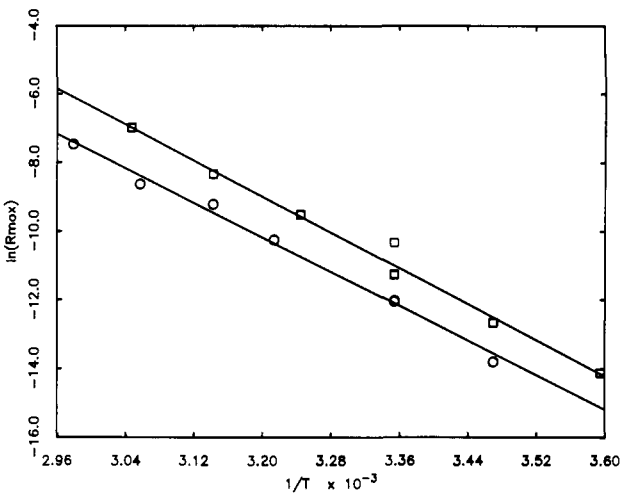

Figure 6. Temperature dependence of photoinitiated formate decomposition by $Cr(CO)_6$ (□) and $W(CO)_6$ (○). R_{max} is the asymptotic limit of the rate with respect to formate concentration (see Figure 2). The phenomenological activation energies are 26.0 ± 1.4 and 24.8 ± 0.8 kcal mol^{-1} for $Cr(CO)_6$ and $W(CO)_6$, respectively.

tocatalytic hydrogen production increases with temperature. As shown by Figure 6, this temperature dependence fits well to an Arrhenius expression. The phenomenological activation energies are 26.0 ± 1.4 and 24.8 ± 0.8 kcal/mol for Cr and W, respectively. Note that these values are considerably less than those found for wholly thermal catalysis (32, 35, and 35 kcal/mol for Cr, Mo, and W, respectively.[4a]

Discussion

Introduction: Expected Kinetics of the Water Gas Shift Cycle. As shown in Figure 2, the rate of hydrogen production in the photoinitiated system exhibits saturation in formate concentration. Such behavior is typical of catalytic mechanisms that involve the binding of one substrate (S) molecule to the catalyst (C) and subsequent conversion to product (P), regardless of the number of intermediates.

$$C + S \rightleftharpoons (CS)_1 \rightleftharpoons (CS)_2 \rightleftharpoons \cdots \rightleftharpoons C + P \quad (4)$$

Any mechanism of the form of reaction 4 will yield a steady-state rate law of the type[11,12]

$$r = d[P]/dt = \alpha[S]/(\beta + [S]) \quad (5)$$

in which

$$R_{max} = \lim_{[S]\to\infty} r = \alpha \quad (6)$$

and α and β are constants with respect to [S].

Equation 5 can be transformed to a convenient form

$$[S]/r = \beta/\alpha + [S]/\alpha \quad (7)$$

whereby a plot of $[S]/r$ vs. [S] yields a straight line, the slope of which is the inverse of R_{max}. As shown by Figure 7 and Table II, such plots of $[HCO_2^-]/r$ vs. $[HCO_2^-]$ for our systems display very good linearity, confirming that a mechanism as in eq 4 in which formate constitutes a substrate is operative.

Table II. Linearized Formate Saturation Data with Variable Temperature and Water Concentration[a]

pre-catalyst	entry	T, °C	$[H_2O]$, M	10^{-5} × slope,[b] m	10^{-3} × intercept,[c] b	corr[d]
$W(CO)_6$	1	25.0	8.35	2.2	8.1	0.998
	2	25.0	5.57	1.7	4.5	0.9996
	3	25.0	5.57	1.7	5.0	0.998
	4	25.0	5.57	1.7	5.4	0.99
	5	25.0	2.79	1.3	3.1	0.998
	6	25.0	2.79	1.8	4.7	0.999
	7	25.0	2.79	1.7	2.9	0.9994
	8	25.0	2.01	1.7	5.9	0.995
	9	25.0	2.01	1.7	5.8	0.9996
	10	25.0	0.557	1.3	2.1	0.997
	11	25.0	0.111	1.2	1.9	0.995
	12	62.5[e]	5.57	0.018	0.052	0.98
	13	54.0	5.57	0.056	0.094	0.98
	14	45.0	5.57	0.10	0.44	0.992
	15	38.0	5.57	0.28	0.97	0.997
	16	15.0	5.57	9.9	27	0.992
$Cr(CO)_6$	17	25.0	8.35	7.8	7.7	0.97
	18	25.0	5.57	5.1	6.2	0.98
	19	25.0	5.57	7.8	4.7	0.98
	20	25.0	5.57	7.8	4.2	0.995
	21	25.0	2.79	3.0	2.4	0.99
	22	25.0	2.79	3.7	3.6	0.96
	23	25.0	2.01	3.8	2.2	0.995
	24	25.0	2.01	3.2	2.3	0.999
	25	25.0	2.01	3.0	2.8	0.97
	26	25.0	5.57	2.0	2.1	0.999
	27	25.0	0.111	1.9	1.8	0.998
	28	55.0	5.57	0.11	0.19	0.96
	29	45.0	5.57	0.42	0.50	0.96
	30	35.0	5.57	1.4	1.4	0.99
	31	15.0	5.57	32	19	0.99
	32	5.0	5.57	140	170	0.97

[a] Each entry corresponds to a run of five formate concentrations (typically 7×10^{-3} to 0.2 M). [b] See eq 7 and 16 in text. [c] See eq 7 and 19 in text. [d] Correlation coefficient for the linear least-squares fit for five samples of varying formate concentration. [e] The error on the temperature here is ±1 °C.

The mechanism proposed by King et al.[4a] (Scheme I) for the thermally catalytic water gas shift reaction contains the necessary formate binding step and thus should show saturation in formate. The rate law constructed from the data, however, does not fit the form of eq 5.

As mentioned above, the apparent (unsaturated) linearity of the rate in formate concentration observed by King et al. reflects the sensitivity of their kinetic system to dissociative initiation. A

(11) Hammes, G. G. "Enzyme Catalysis and Regulation"; Academic Press: New York, 1982; p 41. One exception is if the substrate can also act as an inhibitor. This has been observed in two separate ethylene hydrogenation systems (see ref 12).

(12) (a) Miller, M. E.; Grant, E. R. "Laser initiated homogeneous catalysis: kinetics of elementary reactions", In "Applications of Lasers to Industrial Chemistry"; Woodin, R. L., Kaldor, A., Eds.; Proc. SPIE 458, 1984; p 154. Miller, M. E.; Grant, E. R. *J. Am. Chem. Soc.* **1984**, *106*, 4635. (b) Doi, Y.; Tamura, S.; Koshizuka, K. *J. Mol. Catal.* **1983**, *19*, 213.

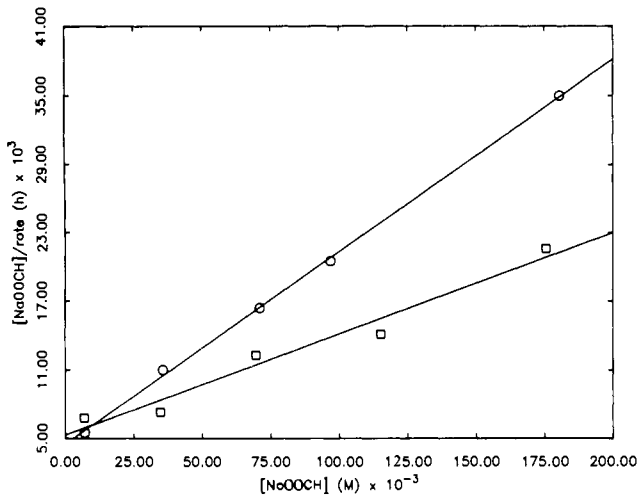

Figure 7. Linearized saturation plot of $[NaO_2CH]$/rate vs. $[NaO_2CH]$ for $Cr(CO)_6$ (□) and $W(CO)_6$ (○) at 25.0 °C. The data are that of Figure 2. A linear dependence is predicted by eq 7 and 12. The inverse of the slope of this plot gives R_{max}.

Scheme II

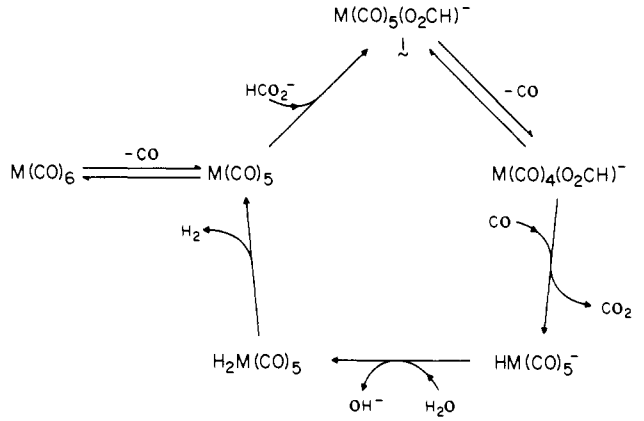

full steady-state analysis of the mechanism as written in Scheme I yields a rate law of the form[13]

$$r = \frac{[M(CO)_6][HCO_2^-]}{(1/k_b)\{(k_{-a}[CO]/k_a) + 1\} + ([HCO_2^-]/k_c)} \quad (8)$$

At high temperatures, such as those required for efficient thermolysis of $M(CO)_6$, k_c, for the formate binding step within the cycle, could well be large compared with k_a, for decarboxylation, thereby reducing eq 8 to eq 2. However, at lower temperatures, or sufficiently high formate concentration, saturation should be expected.

As a matter of fact, in the thermal data[4a] one can find evidence for saturation, which appears in the extremes of the dependence of the rate on base concentration. (Base concentration transforms to formate concentration by the following fast and strongly forward equilibrium: $OH^- + CO \rightleftharpoons HCO_2^-$). Thus, as an important starting point in the analysis of the kinetics of our photochemically initiated system, we recognize clear parallels with the mechanism and kinetics of water gas shift by group 6 carbonyls. In the present case, photolytic preparation of the active catalyst[14] turns kinetic attention away from the initiation step to focus on the rate processes of the catalytic cycle itself. We proceed now to analyze the kinetics of these rate processes with the objective of characterizing the key elementary steps of homogeneous group 6 carbonyl-catalyzed water gas shift.

Scheme III

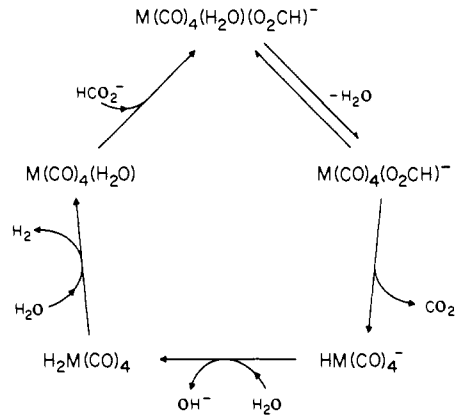

Preceding Decoordination: Inhibition by CO and H_2O. Finding that $M(CO)_5(O_2CH)^-$ rapidly exchanges labeled CO and decarboxylates slower in the presence of added CO, Darrensbourg and Rokicki[8] proposed reversible decoordination preceeding decarboxylation, eq 3. The underlying hypothesis is that hydride migration requires a vacant coordination site. Incorporating this key element into the mechanism sketched by Scheme I, we obtain Scheme II.

On the basis of this mechanism, following the logic of the previous section, our experiment should exhibit saturation behavior with respect to formate. The same should be expected with respect to the second substrate, water. Finally, in parallel to the behavior observed by Darensbourg and Rokicki, we should expect inhibition of the cycle by CO.

Formate saturation is observed (Figure 2); however, we find no detectable inhibition of catalytic turnover by CO (Figure 4), and rather than rate enhancement (to saturation) by increasing water concentration, we find strong inhibition of hydrogen evolution by H_2O (Figure 3).

This apparent disparity between the kinetic behavior of our photocatalytic system and that predicted by Scheme II can readily be explained. A substantial and kinetically significant difference exists between our functioning water gas shift system and the model system employed by Darensbourg and Rokicki to study decarboxylation.

This latter system, the results from which we used to construct Scheme II, is anhydrous. Active water gas shift systems, whether thermal or photochemical, have high water concentrations. Even at the highest CO overpressures (29 psi) used in the present CO inhibition experiments, the concentration of CO in solution is no more than 2×10^{-2} M.[15-17] This is some 300 times less than the usual water concentration in our system and 30 times lower than that typical of thermally induced water gas shift.[4a] At these relative concentrations we can expect diffusion-controlled associative recombinations of coordinatively unsaturated species to be dominated by reaction with water. Thus, a preceding reversible decoordination in CO will rapidly convert to one in H_2O, yielding the mechanism in Scheme III for the inhibitory effect of water.

This mechanism, which features a succession of four 16-electron intermediates, is unrealistic for a reaction in solution. In our reaction system the overwhelming concentration of oxygen donors methanol (24 M) and water (6 M) ensures that the lifetime of any unsaturated species will be very short compared to the overall rate of reaction. Matrix studies show that unsaturated metal carbonyl complexes bind rare gases and methane,[18] and from picosecond laser flash photolysis experiments we know that metal

(13) In deriving this rate law, we assume that the rate of reaction with water and the rate of reductive elimination of H_2 are both fast with respect to decarboxylation (see below in text).

(14) Photoinitiated formate decomposition by the group 6 hexacarbonyls has been previously reported. See ref 4b and also: King, A. D.; King, R. B.; Sailers, E. L., III. *J. Am. Chem. Soc.* **1981**, *103*, 1867.

(15) The average Bunsen coefficient for CO solubility in pure methanol is 0.1796 (see ref 16). This can be converted to the Henry's law constant (see ref 17) to give $[CO] = (1.1 \times 10^{-5})P_{CO}$ torr.

(16) Washburn, E. D., Ed. "International Critical Tables"; McGraw-Hill: New York, 1928; Vol. III, p 265.

(17) Battino, R.; Clever, H. L. *Chem. Rev.* **1966**, *66*, 407.

(18) Perutz, R. M.; Turner, J. J. *J. Am. Chem. Soc.* **1975**, *97*, 4791.

Scheme IV

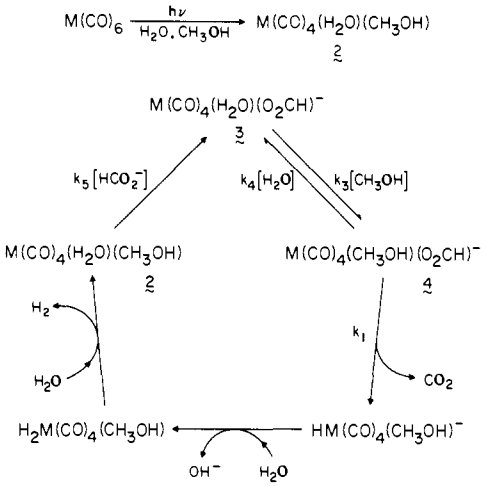

carbonyl–solvent complexes form within 25 ps of photolysis.[19]

Kelly and co-workers suggest that UV photolysis of $Cr(CO)_6$ in the presence of methanol yields the bis-methanol complex $Cr(CO)_4(CH_3OH)_2$.[20] By analogy, we assume that photolysis in our system produces the methanol–water complex **2** ($M(CO)_4(H_2O)(CH_3OH)$). Thus, entering the catalytic cycle with $M(CO)_4(H_2O)(CH_3OH)$, and writing all association reactions (including hydride migration) as methanol displacements, we reconstruct Scheme III as Scheme IV.[21]

Rate Law for Photoinitiated Catalysis of the Water Gas Shift Reaction. The kinetics of this mechanism are simplified by some obvious differences in reaction rates. Reactions that consume water must be exceedingly fast because, even at the lowest water concentrations studied, we fail to see a reduction in rate with decreasing $[H_2O]$: a trace of water is sufficient to achieve saturation in these steps. This conclusion, based on kinetic evidence, is supported by the relative difficulty with which comparable intermediates such as $HM(CO)_5^-$ and $H_2M(CO)_3(PR_3)_2$ are observed in other experiments (only in dry solvents for the former[8,27] and in a hydrogen-enriched atmosphere for the latter[22]).

We can, therefore, regard the postulated intermediates $HM(CO)_4(CH_3OH)^-$ and $H_2M(CO)_4(CH_3OH)$ to be kinetically insignificant and take the rate constant for decarboxylation (k_1) to characterize the transformation from the formate complex, $M(CO)_4(CH_3OH)(O_2CH)^-$, to the solvated tetracarbonyl, $M(CO)_4(H_2O)(CH_3OH)$. The irradiation period is short (≈3 min) compared to the length of the experiment (>3 h). Thus we consider only the time after photolysis and assume a constant total active catalyst concentration (C_t).

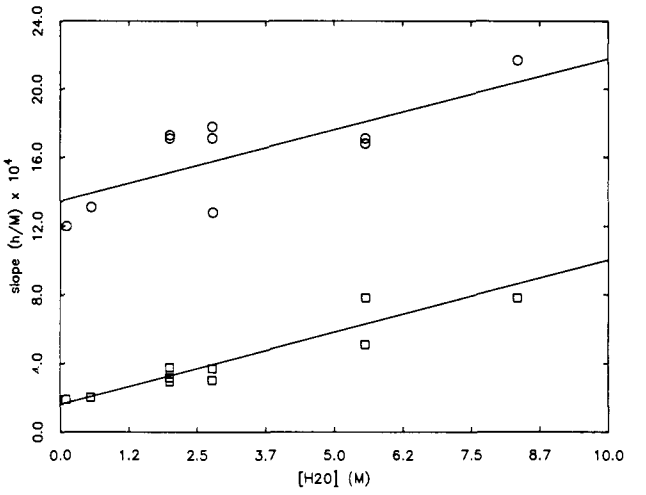

Figure 8. Water dependence of the slope of $[NaO_2CH]$/rate vs. $[NaO_2CH]$ plots for $Cr(CO)_6$ (□) and $W(CO)_6$ (○) at 25.0 °C. A linear dependence is predicted by eq 10 and 12.

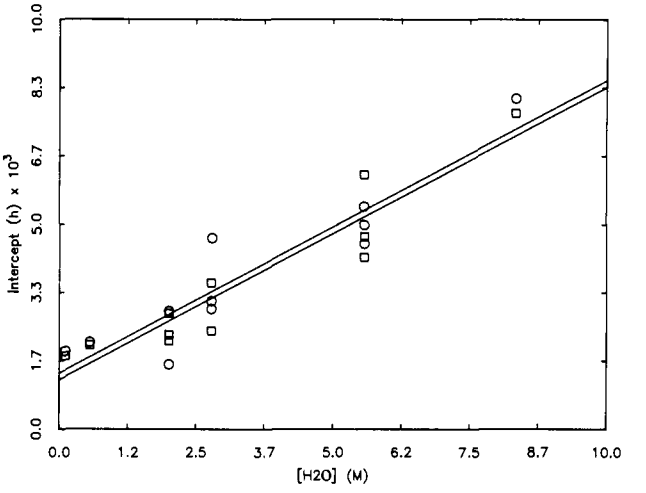

Figure 9. Water dependence of the intercept of $[NaO_2CH]$/rate vs. $[NaO_2CH]$ plots for $Cr(CO)_6$ (□) and $W(CO)_6$ (○) at 25.0 °C. A linear dependence is predicted by eq 12.

Taking these simplifications in conjunction with the steady-state assumption for all intermediates yields the following rate law for hydrogen production

$$r = \frac{d[H_2]}{dt} = \frac{k_1 C_t [HCO_2^-]}{\left\{\frac{K_w[H_2O]}{[CH_3OH]} + \frac{k_1}{k_3[CH_3OH]} + 1\right\}[HCO_2^-] + \frac{k_1}{k_5}} \quad (9)$$

where $K_w = k_4/k_3$ is the water coordination/decoordination equilibrium constant. Note that this rate expression calls for saturation in formate and inhibition by water, in at least qualitative accord with the data.

Equation 9 can be linearized to give

$$\frac{[HCO_2^-]}{r} = \left\{\frac{K_w[H_2O]}{[CH_3OH]} + \frac{k_1}{k_3[CH_3OH]} + 1\right\}\frac{[HCO_2^-]}{k_1 C_t} + \frac{1}{k_5 C_t} \quad (10)$$

Equation 10 predicts that slopes obtained in a plot of $[HCO_2^-]/r$ vs. $[HCO_2^-]$ will increase linearly with $[H_2O]$.[23] Plots of such sets of slopes against water concentration are shown for Cr and W in Figure 8. The good linearity of these plots confirms the coordination/decoordination mechanism for water inhibition of

(19) Welch, J. A.; Peters, K. S.; Vaida, V. *J. Phys. Chem.* **1982**, *86*, 1941.
(20) Kelly, J. M.; Bent, D. V.; Hermann, H.; Schulte-Frohlinde, D.; Koerner von Gustorf, E. *J. Organomet. Chem.* **1974**, *69*, 259.
(21) If formate complexation is made reversible then a quadratic term in water concentration arises in the rate law. Our data do not support a higher order water concentration dependence.
(22) Kubas, G. J.; Ryan, R. R.; Swanson, B. I.; Vergamini, P. J.; Wasserman, H. J. *J. Am. Chem. Soc.* **1984**, *106*, 451.
(23) Strictly speaking, one cannot change $[H_2O]$ without changing $[CH_3OH]$. However, methanol is present in such excess that its variation is negligible compared with its average concentration.
(24) Merrifield, J. H.; Gladysz, J. A. *Organometallics* **1983**, *2*, 782.
(25) At low catalyst conversions (low number of laser pulses), both absorbance and rate of hydrogen production track linearly the number of laser pulses confirming a first-order dependence on active catalyst concentration. Separate formate dependence experiments at half the normal irradiation period show that the slope and intercept (with respect to formate) of eq 15 increase by a factor of 2 as predicted. This also supports a first-order dependence of the rate on active catalyst concentration.
(26) A possible cause of the observed saturation of the reaction rate and visible absorbance with respect to laser pulses is complete absorption of laser light by intensely absorbing photoproducts (inner filter effect). However, UV–vis absorption measurements show that the absorbance at 337 nm *decreases* with photolysis.
(27) (a) Darensbourg, M. Y.; Deaton, J. C. *Inorg. Chem.* **1981**, *20*, 1644. (b) Darensbourg, M. Y.; Slater, S. *J. Am. Chem. Soc.* **1981**, *103*, 5914. (c) The tendency to dimerize is pronounced in molybdenum hydride systems (see ref 27b). Our preliminary studies of photoinitiated WGSR catalysis using $Mo(CO)_6$ showed very low activity accompanied by the formation of a precipitate.

Scheme V

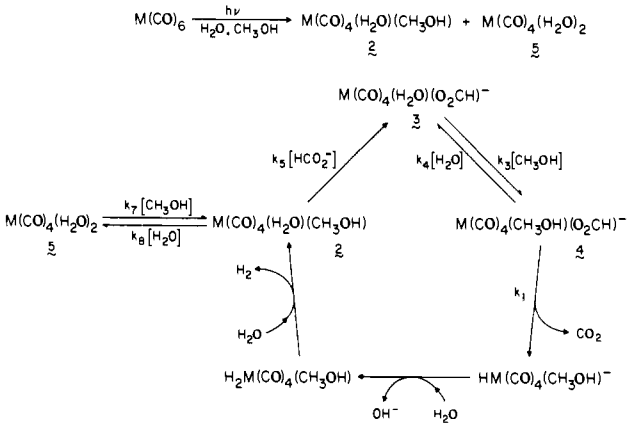

water gas shift. Equation 10 also predicts that for a given system the intercepts of plots of $[HCO_2^-]/r$ vs. $[HCO_2^-]$ will be independent of water concentration. When we plot the collection of such intercepts against $[H_2O]$, we find that they are not constant but rather increase linearly with $[H_2O]$ (Figure 9). Within experimental uncertainty both W and Cr show identical behavior.

Now, an increasing intercept in the $[HCO_2^-]/r$ plot corresponds to a decreasing rate. Thus, we have established that a second pathway exists for water inhibition, a pathway that is not included in Scheme IV.

In the development above, we simplified the kinetics by ignoring bis-water and bis-methanol complexes as possible solvated photoproducts. We expect on the basis of binding strength arguments that the stabilities of the three possible photoproducts will vary as $M(CO)_4(H_2O)_2 > M(CO)_4(H_2O)(CH_3OH) > M(CO)_4(CH_3OH)_2$. Thus it is logical to construct our mechanism in terms of the dominant species $M(CO)_4(H_2O)_2$ and $M(CO)_4(H_2O)(CH_3OH)$. Assuming that the rate of reaction of formate with $M(CO)_4(H_2O)_2$ is slow relative to that with $M(CO)_4(H_2O)(CH_3OH)$, we rewrite Scheme IV as Scheme V.

Applying the same assumptions to Scheme V as used to derive eq 9 from Scheme IV yields the following rate law

$$r = \{k_1C_t[HCO_2^-]\}/\left[\left\{\frac{K_w[H_2O]}{[CH_3OH]} + \frac{k_1}{k_3[CH_3OH]} + 1\right\} \times [HCO_2^-] + \frac{k_1}{k_5}\left\{\frac{K_w'[H_2O]}{[CH_3OH]} + 1\right\}\right] \quad (11)$$

in which $K_w' = k_8/k_7$ and other rate constants are as defined above.

In its linearized form eq 11 is

$$\frac{[HCO_2^-]}{r} = \left\{\frac{K_w[H_2O]}{[CH_3OH]} + \frac{k_1}{k_3[CH_3OH]} + 1\right\}\frac{[HCO_2^-]}{k_1C_t} + \frac{1}{k_5C_t}\left\{\frac{K_w'[H_2O]}{[CH_3OH]} + 1\right\} \quad (12)$$

and by virtue of the second term we have precisely the linear dependence of the intercept on water concentration found in the data. As with the first term, which reflects the water dependence in the slope, we have in this dependence the equilibrium constant (here K_w') and, to within a factor of the catalyst concentration, a rate constant. To separate these terms and extract numbers for each of the rate and equilibrium constants of this catalytic system, we need to both simplify eq 12 and develop a means to estimate the absolute catalyst concentration, C_t. We proceed first to simplify the kinetics.

Simplification of the Rate Law. The magnitude of hydrogen isotope effects for Cr and W cycles point to a key simplification that enables the separation of terms in eq 12. When the formate saturation experiment is repeated with all protons replaced by deuterium, R_{max} is found to decrease substantially at 25 °C: $R^H_{max}/R^D_{max} = 3.4 \pm 0.9$ and 4.4 ± 0.2 for Cr and W, respectively. Thus the rate-limiting step under conditions of saturation in formate must involve the movement of H(D). As discussed above, proton transfer and reductive elimination of H_2 should be fast, leaving decarboxylation/hydride migration as the most likely source of the kinetic isotope effect. This conclusion is supported by work on the decarboxylation of $(\eta^5\text{-}C_5H_5)Re(NO)(PPh_3)(O_2CH)$ which, in experiments that isolate the hydrogen migration/CO_2 loss step, establishes a primary isotope effect for DCO_2^- compared with HCO_2^-.[24] Then if we can assume that the decarboxylation of $M(CO)_4(CH_3OH)(O_2CH)^-$ limits the rate of the formate-saturated cycle, it follows that the preceding step (k_3) must be fast. If the equilibrium constant for water–methanol exchange favors water (an expectation in accord with the hard/soft acid–base principle and confirmed by experimental data below), then the rate constant for the back reaction (k_4) must be even greater. Thus we can regard water–methanol exchange as a fast preceding equilibrium, with

$$k_1 \ll k_3[CH_3OH] \quad (13)$$

This assumption is seen to be consistent with our observation of photoacceleration of the water gas shift cycle when one considers the likely effect of light on the position of this equilibrium. Irradiation induces ligand loss. In an environment rich in methanol, particularly if the water–formate complex **3** is dominant, light will shift the equilibrium to a new photostationary state, richer in the methanol coordinated precursor to hydride shift/decarboxylation, **4**.

Adopting the assumption of eq 13 we can simplify eq 11 as follows

$$r = \frac{k_1C_t[HCO_2^-]}{\left\{\frac{K_w[H_2O]}{[CH_3OH]} + 1\right\}[HCO_2^-] + \frac{k_1}{k_5}\left\{\frac{K_w'[H_2O]}{[CH_3OH]} + 1\right\}} \quad (14)$$

which linearizes to

$$\frac{[HCO_2^-]}{r} = \left\{\frac{K_w[H_2O]}{[CH_3OH]} + 1\right\}\frac{[HCO_2^-]}{k_1C_t} + \frac{1}{k_5C_t}\left\{\frac{K_w'[H_2O]}{[CH_3OH]} + 1\right\} \quad (15)$$

Examination of eq 15 shows that the formate concentration dependence obtained as a function of water concentration will give independent values for k_1C_t, k_5C_t, $K_w/[CH_3OH]$, and $K_w'/[CH_3OH]$. From eq 15 the slope of a plot of $[HCO_2^-]/r$ vs. $[HCO_2^-]$ will be given by

$$m = \frac{1}{k_1C_t}\left\{\frac{K_w[H_2O]}{CH_3OH]} + 1\right\} \quad (16)$$

If we plot a collection of such slopes (m), obtained for various choices of water concentration, vs. $[H_2O]$ we obtain a new slope and intercept (m_m and b_m, respectively)

$$m_m = \frac{K_w}{k_1C_t[CH_3OH]}; \quad b_m = \frac{1}{k_1C_t} \quad (17)$$

and the ratio of m_m to b_m determines $K_w/[CH_3OH]$

$$m_m/b_m = K_w/[CH_3OH] \quad (18)$$

The intercept of a plot of $[HCO_2^-]/r$ vs. $[HCO_2^-]$ is expressed by eq 15 as

$$b = \frac{1}{k_5C_t}\left\{\frac{K_w'[H_2O]}{[CH_3OH]} + 1\right\} \quad (19)$$

As before a collection of intercepts (b) plotted against $[H_2O]$ will yield new slope and intercept

$$m_b = \frac{K_w'}{k_5C_t[CH_3OH]}; \quad b_b = \frac{1}{k_5C_t} \quad (20)$$

and their ratio determines $K_w'[CH_3OH]$

$$m_b/b_b = K_w'/[CH_3OH] \quad (21)$$

Plots confirming the linearity of eq 16 and 19 over the range of our experiments are given as Figures 8 and 9. From these plots

Table III. Equilibrium Constants and Free Energies of Reaction Derived from Linear Fits to the Water Concentration Data

M	$10^{-4} \times b_m$,[a] M^{-1} h	$10^{-3} \times m_m$,[a] M^{-2} h	$10^{-3} \times b_b$,[b] h	$10^{-2} m_b$,[b] M^{-1} h
Cr	1.6 ± 0.5	8 ± 1	1.2 ± 0.4	7.0 ± 0.9
W	13 ± 1	8 ± 2	1.4 ± 0.4	7 ± 1
M	K_w[c]	$\Delta G°_{298}$, kcal	K_w'[d]	$\Delta G°_{298}'$, kcal
Cr	12 ± 5	−1.5 ± 0.3	14 ± 5	−1.6 ± 0.2
W	1.4 ± 0.5	−0.2 ± 0.2	12 ± 5	−1.5 ± 0.2

[a] As defined by eq 16 and 17. [b] As defined by eq 19 and 20. [c] $K_w = k_4/k_3$ at 25.0 °C for the water equilibrium preceding decarboxylation and is calculated from eq 18 with use of the mean methanol concentration of 23.5 M.[23] [d] $K_w' = k_8/k_7$ at 25.0 °C for the water equilibrium preceding entry into the cycle and is calculated from eq 21 with use of the mean methanol concentration of 23.5 M.[23]

Table IV. Rate Constants and Concentration of Active Catalyst

M	10^4[M(CO)$_6$], M	R_{expt}/R_∞[a]	$10^4 C_t$, M	$10^4 k_5$,[b] M^{-1} s^{-1}	$10^6 k_1$,[c] s^{-1}
Cr	1.7	0.9 ± 0.2	1.5 ± 0.3	12 ± 8	116 ± 43
W	18	0.5 ± 0.1	9.0 ± 1.8	3 ± 1	2.3 ± 0.2

[a] These data are from experiments with normal catalyst concentrations whereas the data of Figure 10 are for reduced catalyst concentrations for technical reasons. [b] The rate constant for formate binding at 25.0 °C as calculated from eq 20. [c] The rate constant for decarboxylation at 25.0 °C as calculated from eq 17.

we obtain slope and intercept parameters m_m, b_m, m_b, and b_b tabulated in Table III. Multiplying the ratios of m_m to b_m and m_b to b_b by the average methanol concentration, 23.5 M, yields K_w and K_w' for Cr and W as listed in Table III. Note that all of the water–methanol exchange equilibria lie toward the H_2O complex, a finding that supports the supposition expressed by eq 13. The origin of the much larger dependence of R_{max} on [H_2O] for Cr over W is also now evident in the relative magitudes of K_w for Cr compared with W. For Cr, the $M(CO)_4(H_2O)(O_2CH)^-$ complex, **3**, is much more so the favored component of the pair. Thus the equilibrium concentration of the active component is more sensitive to an increase in [H_2O], as established mathematically by the magnitude of K_w as a coefficient of [H_2O] in the denominator of eq 14.

Intercept terms b_m and b_b contain information about k_1 and k_5. To extract absolute rate constants from these terms requires knowledge of the laser produced active catalyst concentration. Estimate is made of this quantity as follows.

Catalyst Concentration, C_t. Determination of C_t presents a significant problem because there exists no direct means to measure the concentration of active catalyst generated by photoconversion of $M(CO)_6$. However, an estimate can be made by examining the dependence of the reaction rate and visible absorbance on the number of photons absorbed, as both of these quantities should be proportional to C_t. Figure 10 shows that these quantities do obey the same functional dependence on the number of laser pulses. As more photons are absorbed by the sample, both the rate of hydrogen production and visible absorbance increase and approach an asymptotic limit.[25]

This phenomenon offers a particularly simple means to estimate C_t for any number of laser pulses: Under the assumption of no side products in the conversion of $M(CO)_6$ to catalyst, the asymptotic limit in either the visible absorbance or catalytic rate curves corresponds to a condition in which C_t is equal to the original $M(CO)_6$ concentration. For the irradiation time typical of these experiments, we calculate the catalyst concentration to be about half the original $M(CO)_6$ concentration for W, while for Cr we estimate near-total conversion (Table IV).[26]

These estimates are, of course, strictly upper bounds. Any process that diverts photolyzed metal carbonyl fragments from the catalytic cycle will cause the asymptotic limit to be reached with less than the full, original $M(CO)_6$ concentration as active catalyst. Catalyst loss mechanisms do exist. Over very long periods of time we observe the rate of hydrogen production at constant formate to decline slightly. This problem is most severe

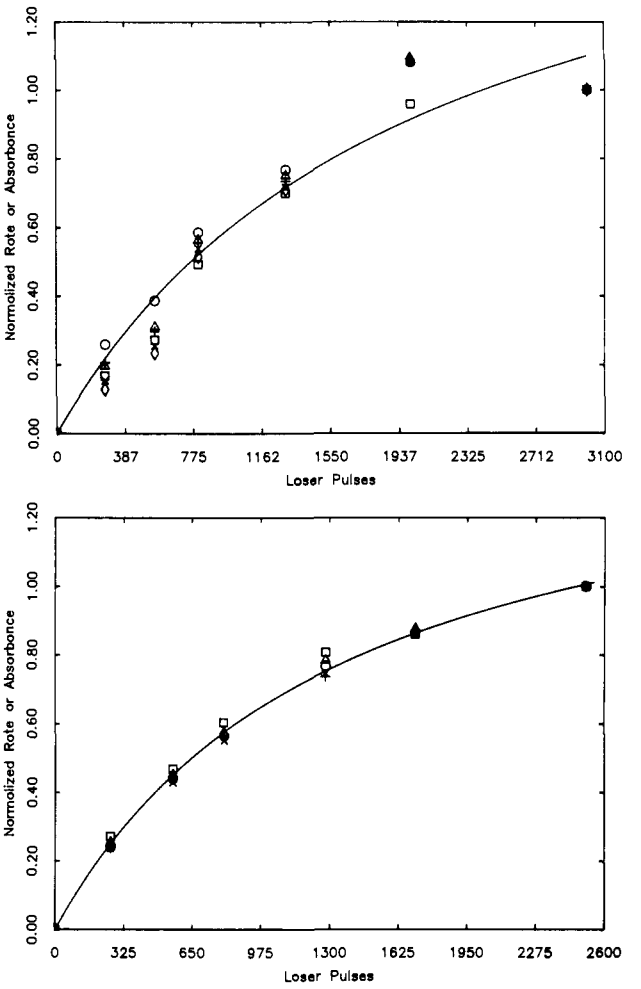

Figure 10. Determination of catalyst concentration (C_t): (a, top) Cr(CO)$_6$ and (b, bottom) W(CO)$_6$. The rate of hydrogen production (□) and the visible absorbance (○, △, ×, +, ◇) (λ_{max} = 432 and 408 nm for Cr and W, respectively), each normalized to the value at the maximum number of laser pulses, are plotted against the number of laser pulses used. Some reduction in visible absorbance is observed with time as reflected by the scatter in the data.

for the Cr system at high temperature. At all temperatures we find that acceptably constant long-term H_2 evolution can be achieved only for reduced initial chromium carbonyl concentrations (ten times lower than that for tungsten). On the basis of this finding, we suspect that the problem of catalyst degradation can be traced to the formation of dinuclear (or higher) clusters. A likely candidate is μ-H[M(CO)$_5$]$_2^-$ which has been observed to be quite stable.[27]

For all runs in which kinetic data are taken, catalyst concentrations are set so that H_2 production is constant over the entire experiment. In assessing the validity of our assumption in using Figure 10 to determine C_t, there remains then only short term catalyst loss mechanisms, such as branching on photolysis, to consider. A check on this assumption, which is that of unit quantum yield for catalyst production, can be made by calculating the maximum possible concentration based on the number of photons incident on the sample. On the basis of separate solution actinometry, we know the maximum concentration of catalyst possible if all incident photons are absorbed by $M(CO)_6$ and the quantum yield for production of catalyst is unity: 8×10^{-4} M (Table IV). For W this upper limit corresponds precisely with the estimate obtained by use of Figure 10. For Cr, the hexacarbonyl concentration is ten times lower and apparently not all the light incident is absorbed, reducing the value of this upper limit. However, this does not affect the validity of the method of Figure 10, and on the basis of the apparent accuracy of this method for W, we assume the calculated value of C_t listed in Table IV for Cr is accurate as well.

Table V. Consistency Check on Rate Constants

catalyst	$[H_2O]$, M	$[NaO_2CH]$, M	10^6rate,[a] M h^{-1}	10^6k_1,[b] s^{-1}
$W(CO)_6$	0.111	0.158	7.8	2.4
	0.557	0.172	5.4	1.7
	2.01	0.169	5.4	1.9
	2.01	0.183	5.3	1.8
	2.79	0.170	5.3	1.9
	2.79	0.162	4.8	1.7
	2.79	0.164	6.6	2.4
	5.57	0.167	4.9	2.0
	5.57	0.183	5.3	2.2
	5.57	0.181	5.2	2.1
	8.35	0.149	3.7	1.7
				$\bar{x} \pm s = 2.0 \pm 0.3$
$Cr(CO)_6$	0.111	0.178	35	69
	0.557	0.177	31	74
	2.01	0.168	21	79
	2.01	0.173	22	83
	2.01	0.173	29	110
	2.79	0.131	15	67
	2.79	0.181	22	99
	5.57	0.223	13	93
	5.57	0.176	9.2	65
	5.57	0.180	9.6	68
	8.35	0.161	76	74
				$\bar{x} \pm s = 80 \pm 15$

[a] The observed rate of hydrogen production at 25.0 °C and the highest formate concentration used. [b] Calculated from eq 22. These values should be compared to those in Table III. As expected, these are consistently lower since the rate is not at the asymptotic limit (R_{max}).

Absolute Rate Constants for Formate Attack and Decarboxylation within the Catalytic Cycle for Water Gas Shift. Having obtained estimates of C_t for Cr and W systems, we can calculate values for k_1 (decarboxylation) and k_5 (substitution by formate) by eq 17 and 20. These results are listed in Table IV. Note that the values obtained for k_5 are comparable for Cr and W, whereas k_1 for Cr is 50 times larger than that for W.

The values of k_1 can be checked for internal consistency by back calculating values for k_1 from the equation for R_{max}

$$R_{max} = \frac{k_1 C_t}{\left\{\frac{K_w[H_2O]}{[CH_3OH]} + 1\right\}} \qquad (22)$$

using the rate of H_2 evolution at the highest formate concentration to represent R_{max}, together with the calculated values of $K_w/[CH_3OH]$, the water concentration, and the estimated catalyst concentration (C_t). When this is done at each water concentration for both Cr and W, we find good agreement with the values calculated from b_m (see Table V). The agreement is better for W than for Cr since the rate at the highest formate concentration ($\simeq$0.2 M) is closer to R_{max} (see Figure 2). Note that this does not check the value of C_t as both methods require the estimated value.

Activation Energy for the Catalytic Cycle. Our data provide a measure of the temperature dependence of R_{max}. To place this in a context of Arrhenius parameters for elementary reactions we must examine the predicted temperature dependence of R_{max} from our mechanism. From eq 22 we can construct the phenomenological activation energy as

$$E_a = -R\frac{\partial \ln (R_{max})}{\partial(1/T)} = E_1 - \frac{\Delta H}{\left\{\frac{[CH_3OH]}{K_w[H_2O]} + 1\right\}} \qquad (23)$$

where E_1 is the activation energy for decarboxylation and ΔH is the reaction enthalpy associated with K_w. From Table III the values of $\Delta G°_{298}$ corresponding to the listed K_w are −1.5 and −0.2 kcal/mol for Cr and W, respectively. It is likely that $\Delta S°_{298} \approx 0$, then $\Delta G°_{298} \approx \Delta H°_{298}$ and the temperature dependence of the equilibrium constant (K_w) is small. Under this assumption and using the values of K_w found for 25.0 °C, we calculate $\Delta H/\{([CH_3OH]/K_w[H_2O]) + 1\}$ to be −1.1 and −0.06 kcal/mol while E_a is found to be 26.0 and 24.8 kcal/mol for Cr and W, respectively. Thus to a first approximation we can neglect the second term in eq 23 and equate the phenomenological activation energies to that for the decarboxylation step. As an interesting comparison, the activation enthalpy for a similar reaction, decarboxylation of $(\eta^5\text{-}C_5H_5)Re(NO)(PPh_3)(O_2CH)$, is 26.8 ± 0.6 kcal/mol.[24] By contrast, recall that the thermal activation energies are about 35 kcal/mol. Photolysis removes a barrier that is some 10 kcal/mol higher than the largest barrier in the catalytic cycle.

Conclusions and Relevance of Photocatalytic Formate Decomposition to Thermal Water Gas Shift. We have constructed a comprehensive picture of the kinetics of the group 6 photocatalytic decomposition of formate/reduction of water (water gas shift cycle). Formate-saturation kinetics have yielded maximum rates (R_{max}) as a function of temperature for chromium and tungsten carbonyl systems. We observe photoacceleration of the cycle by visible light, a result consistent with a reversible decoordination step preceding decarboxylation as predicted by Darensbourg and co-workers.[8] As shown by CO and water dependence studies, however, this decoordination step appears in our H_2O/methanol system as a preceding equilibrium in water–methanol exchange (as opposed to the CO exchange characterized by Darensbourg and co-workers in their anhydrous system). The shift in this equilibrium with increasing H_2O concentration slows the cycle by decreasing the concentration of the precursor, **4**, to rate-limiting decarboxylation. Kinetic evidence suggests that the cycle is carried by a (methanol) solvated metal tetracarbonyl. Also on the basis of kinetic information, we identify a second competitive binding inhibition in H_2O.

By conducting experiments in which we carry the $M(CO)_6$-to-catalyst conversion to completion, we have been able to estimate the active catalyst concentration, C_t, in our kinetic system. This information allows the calculation of absolute rate constants for decarboxylation and attack on the solvated tetracarbonyl complex, **2**, by formate. Isotope effects confirm that the rate-determining step under formate saturation is decarboxylation (accompanied by hydride migration), and temperature-dependent rate data give activation energies for this step for chromium and tungsten carbonyl systems. These measured barriers are some 10 kcal lower than those characteristic of thermal catalysis of water gas shift.

Finally, this brings us again to the question of correspondence between the kinetics and mechanism of the photocatalytic decomposition of formate/reduction of water and that of the thermal catalysis of water gas shift. An alternative mechanism for thermal catalysis of water gas shift by metal carbonyls exists.[3] It proceeds via a metallocarboxylic acid intermediate generated by hydroxide attack at a coordinated CO.

$$M(CO)_n \xrightarrow{OH^-} M(CO)_{n-1}COOH^- \qquad (24)$$

The suggestion has been made that this is the predominant pathway for thermal catalysis of water gas shift by the group 6 metal carbonyls and that photochemical initiation biases the system toward the formate mechanism.[8] However, the most complete thermal data for an active water gas system are inconsistent with this hypothesis. King and co-workers[4a] observe an inverse dependence of the rate on CO pressure. Moreover, the observed thermal rate is independent of the identity of the base (OH^-, $(C_2H_5)_3N$, or HCO_2^-). Neither of these results is predicted by a mechanism that begins with OH^- attack, but they are consistent with one involving coordination of formate, such as Scheme I, originally proposed by King and co-workers.[28]

(28) Reaction 24 for M = Cr, W can be fast relative to formate decomposition ($M(CO)_5O_2CH^- \rightarrow HM(CO)_5^- + CO_2$) in nonaqueous solution[8] and production of H_2 via (24) is faster than the formate route at low temperatures.[29] However, such conditions are not typical of water gas shift systems. At high temperatures ($\approx$150 °C) in aqueous solution, the rates of CO loss from $M(CO)_6$ and the formation and decomposition of formate are all likely to be faster than (24), a supposition which is confirmed by the kinetic data.[4a]

As pointed out by this work, however, Scheme I is incomplete. The requirement for decoordination preceding decarboxylation has been established. Even under thermal water gas shift conditions with its high overpressure of CO, concentrations of H_2O and solvent (CH_3OH) vastly exceed that of CO in solution, and we should expect certain parallels with our photochemical system. Indeed, an inhibitory effect of H_2O has been noted in the thermal system.[4a] Thus, it appears that a mechanism appropriate for the core cycle of the thermal as well as photoinitiated water gas shift reaction is given in this work as Scheme V.

Experimental Section

General. A stock solution of $M(CO)_6$ in 10% H_2O/CH_3OH (v/v) is prepared for each run of five samples. The solubility of metal carbonyl in this polar solvent mixture is very low, and several hours are required for complete dissolution. NaO_2CH is added last, either by volumetric dilution of a stock solution or directly. Degradation, visible as a precipitate, occurs after about a week with these final solutions, and therefore all are used within 24 h of preparation. For irradiation, samples are transferred to a matched set of cylindrical (1.0 in. o.d. × 4 in.) Pyrex cells fitted with Teflon high-vacuum stopcocks and outgassed by bubbling N_2 through the solution followed by 2 freeze–pump–thaw cycles. Complete deoxygenation is found to be critical for reproducible kinetic behavior.

Cells are irradiated with the pulsed output of a Lambda-Physik EMG-101 excimer laser with the N_2 (337 nm) line. This corresponds to an irradiation period of just over 3 min after which samples are kept in the dark for the duration of the experiment (several hours to several days). Pulse energy is 2.4 mJ (accurately measured and held constant), and the pulse width is 5–10 ns.

Temperature is controlled by use of a thermostated water bath (±0.1 °C). For runs at $T > 35$ °C, the reaction is quenched in an ice-water bath for sampling.

Product hydrogen is analyzed on a home-built gas chromatograph equipped with a thermistor detector (Gow-Mac). Separation is achieved by flowing nitrogen carrier gas through a 4 ft (0.125 in. o.d.) Porapak Q column followed by a 12 ft (0.125 in. o.d.) 13× molecular sieve column, all maintained at 40 °C. The columns are backflushed after each analysis to prevent degradation of the molecular sieve. A gas-sampling valve serving an evacuatable injection loop is used to analyze the gas in the cell. Immediately following injection, all gases that remain are evacuated from the cell.

The absolute yield of hydrogen is determined by calibration of the GC for each set of experimental conditions. A capacitance manometer is used to place known amounts of hydrogen in the reaction cells with a blank aliquot of solvent. The inclusion of solvent is critical since it greatly affects the amount of gas sampled.

Quantum yields are determined by ferrioxalate actinometry.[30] To assure constant power for all runs, laser output is continually monitored by a thermopile power meter (Scientech).

All samples are prepared and degassed on a glass vacuum line where absolute pressures are measured with a capacitance manometer (MKS, 0–10 torr) or a bourdon tube gauge (Heise, 0–50 psi). UV–vis spectra are taken on a Hewlett-Packard 8450A spectrometer. Reagent grade methanol (Mallinckrodt), NaO_2CH (99.0%, GFS Chemicals), NaO_2CD (MSD Isotopes, 99% D), CH_3OD (MSD Isotopes, 99% D), and D_2O (Aldrich Gold, 99.8% D) are used as received. Tungsten and chromium carbonyls (Alfa) are purified by vacuum sublimation.

Formate Saturation (Figures 1, 2, and 7). Samples (10.0 mL) are run in sets of five. Held at constant concentration in methanol solution are $Cr(CO)_6$ (1.7×10^{-4} M) or $W(CO)_6$ (1.8×10^{-3} M) and H_2O (10% v/v, 5.57 M). The formate concentration (as NaO_2CH) is varied from about 5×10^{-3} to 0.2 M (the solubility limit). Isotope effect experiments are carried out identically with D_2O, NaO_2CD and CH_3OD. Formate saturation behavior is also characterized in the course of water dependence studies. These are carried out in the manner described above with the addition of variable H_2O concentration over the range from 0.2% (0.11 M) to 15% (8.4 M).

CO Overpressure (Figure 4). Sample and control consisting of (15.0 mL) of hexacarbonyl and formate solution ($[H_2O] = 5.57$ M; and either $[Cr(CO)_6] = 4.79 \times 10^{-4}$ M and $[NaO_2CH] = 0.0886$ M or $[W(CO)_6] = 4.50 \times 10^{-4}$ M and $[NaO_2CH] = 0.0946$ M) are prepared in the manner above. After outgassing, the samples are irradiated and the H_2 production is monitored in the usual way. A base rate for H_2 evolution is established by taking three samples. The test cell is then pressurized with CO (29 psi). To compensate for the separate effect of a large pressure of gas on H_2 sampling, an equivalent pressure of N_2 is added to the control. The visible absorbance is monitored ($\lambda_{max} = 432$ nm for Cr, $\lambda_{max} = 408$ nm for W) over the course of the reaction. The gas (N_2 or CO) is replenished after each subsequent H_2 sampling.

Photoacceleration (Figure 5). Samples consisting of 15.0 mL of hexacarbonyl and formate solution ($[H_2O] = 5.57$ M; and either $[Cr(CO)_6] = 1.66 \times 10^{-4}$ M and $[NaO_2CH] = 0.184$ M or $[W(CO)_6] = 1.79 \times 10^{-3}$ M and $[NaO_2CH] = 0.177$ M) are prepared as above. The cells are thermostated at 22.1 ± 0.3 °C by close contact with a large mass aluminum block (aided by silicone heat sink compound). A thermocouple immersed in the solution monitors the temperature. The base rate is established by taking three H_2 samples. The cell is then irradiated with a 100-W tungsten–halogen lamp filtered by colored glass filter and a cell filled with $CuSO_4/NH_4OH$ solution, which serve to isolate ~10 mW in the 350–500 nm region and to prevent IR heating. Separate control experiments show that visible irradiation, under these conditions, does not induce H_2 production without prior UV irradiation. The rate under continuous visible irradiation is established, and then the rate with the lamp off is redetermined as a check.

Determination of Catalyst Concentration (Figure 10). Special cells designed to withstand liquid nitrogen temperature for outgassing and to allow the parallel measurement of visible absorbance and hydrogen production are employed. The ends consist of 1.0 in. diameter × 0.125 in. thick Pyrex optical windows fused to 4 cm long pieces of 1.0 in. o.d. heavy wall tubing. The rest of the cell is identical with our standard cell. The pathlength of each cell is calibrated by the absorbance of $NaNO_2$-(aq) (354 nm) relative to that in a 1.0-cm cuvette.

Samples (15.0 mL) of hexacarbonyl and formate solution ($[H_2O] = 5.57$ M; and either $[Cr(CO)_6] = 1.67 \times 10^{-4}$ M and $[NaO_2CH] = 0.200$ M, or $[W(CO)_6] = 1.65 \times 10^{-4}$ M and $[NaO_2CH] = 0.186$ M) are prepared as above. After outgassing the background absorbance ($\lambda_{max} = 432$, 408 nm for Cr and W, respectively) is measured, the samples irradiated with an increasing number of pulses (≈200 to ≈3000) at constant energy (1.4 mJ/pulse), and the induced absorbance measured. Hydrogen production and visible absorbance are monitored over ≈30 h.

Acknowledgment. We gratefully acknowledge the support of this work by Koppers Company, Inc.

Registry No. $Cr(CO)_6$, 13007-92-6; $W(CO)_6$, 14040-11-0.

(29) Darensbourg, D. J.; Rokicki, A. *ACS Symp. Ser.* **1981**, *No. 152*, 107.
(30) Calvert, J. G.; Pitts, J. N., Jr. "Photochemistry"; Wiley: New York, 1955; pp 783–786.